AADE-19-NTCE-SPP-06

Modeling Flow Pattern Transition in Co-current Two-Phase Gas-Non-Newtonian Liquid Flow in Vertical Upward Concentric Annulus

Víctor H. Lema and Tan C. Nguyen, New Mexico Institute of Mining and Technology; Eissa Al-Safran, Kuwait University

Abstract

Flowing bottom-hole pressure prediction in Concentric Casing Gas Injection (CCGI) drilling operation using mechanistic models requires the determination of gas-liquid two-phase flow patterns along the annuli. This paper proposes two flow pattern transition models, namely bubble/dispersed bubble (BL/DB), and intermittent/annular (IN/AN) in CCGI upward co-current concentric annuli flow of a gas and pseudo-plastic non-Newtonian liquid two-phase mixture. The effect of shear-thinning rheological behavior and annular geometry were incorporated into the models´ development. Sensitivity analysis was performed to investigate the effect of shear-thinning fluid behavior on both transition boundaries. The results reveal that the shear-thinning behavior of the liquid phase has a significant effect on the transition boundary of BL/DB, but has a minimal effect on the IN/AN transition boundary. The findings of this study improve not only the hydrodynamic predictions in CCGI, but also the performance of the mechanistic models of gas and non-Newtonian liquid mixtures.

Introduction

A technical option to drill thru consolidated and highly depleted oil reservoirs is Concentric Casing Gas Injection (CCGI) which could be classified as a Managed Pressure Drilling (MPD) method. It is potentially suitable to maximize productivity and ultimate recovery by reducing formation damage when drilling through pay zones in mature oil fields without lessen heat transfer and directional control capabilities at downhole conditions.

The design and operational issues of CCGI have been described by previous authors (Mykytiw et al., 2003; Beltran et al., 2010) as well as some field applications of the method in Mexico (Urbieta et al. 2009; Perez-Tellez et al., 2009; Rodriguez et al., 2013).

Practically, it can be assumed that flow is under steady state condition when drilling with a CCGI system and the gas injection point is located in the vertical section as shown in Fig. 1. While using CCGI drilling, a co-current gas-liquid-solid mixture is flowing upwardly inside of the primary annulus above the gas injection point. Unweighted oil-based mud (e.g. invert emulsion) is used as drilling fluid to reduce the bottomhole pressure and hence reduce formation damage and costs associated with drilling fluid losses. In this paper, solid phase is considered part of the liquid phase for modeling flow pattern transitions.

Mechanistic modeling of gas-liquid two-phase flow involves flow pattern definition and flow pattern transition criteria. Gas-liquid two-phase models and flow pattern transition criteria were initially developed for a gas and Newtonian liquid mixture in pipe flow. Only a few comprehensive studies concerning to gas-liquid two-phase upward vertical flow in annuli exist in the literature and they are mainly for Newtonian liquid phase. The goal of this work is to develop flow pattern transition criteria which take into account the shear thinning rheological behavior of unweighted oil-based drilling fluids and the nonlinear shear-stress distribution within the annulus.

Studies of Non-Newtonian fluid flow in an annulus have received much less attention in comparison to Newtonian fluid flow in pipe. Friction factor is the main parameter of interest in most studies. The flow of non-Newtonian fluids in annuli is quite different from the flow in pipes. For pipe flow, zero shear stress and maximum velocity coincide at the center of the pipe while shear stress varies linearly with the distance from the inner wall. For annular flow, flow is not symmetric; shear stress does not decline linearly with the distance from inner walls. The case of laminar flow in concentric annuli has a theoretical solution for stress distribution (Frederick and Bird, 1958), but transitional and turbulent regimes are still without analytical solution universally accepted.

The aim of this paper is to introduce new flow pattern transition criteria that can be applied to improve flowing bottom-hole pressure estimations while drilling with CCGI. Namely, bubble/dispersed bubble (BL/DB), and intermittent/annular (IN/AN) transitions in co-current two-phase flow of a gas and pseudo-plastic non-Newtonian liquid mixture in vertical upward concentric annuli. To support the motivation for this work we added some background and fundamentals at Appendix A as a supplement to the topic of incompressible single-phase flow of power-law fluids through annuli.

Development of models

The bubble/dispersed bubble (BL/DB) transition.

In the present work we followed the same phenomenological description suggested by Taitel et al. (1980) and developed for steady upward gas-liquid (Newtonian) two-phase flow in circular tubes.

Transition occurs at high liquid flow rates with liquid as the continuous phase and gas as the dispersed phase. At turbulent conditions, shear stresses tend to break up the larger bubbles, inhibiting agglomeration and coalescence of bubbles. Then, the transition is dominated for a force balance between turbulent force of the liquid (disruptive force) and surface tension force of the bubbles (restorative force). The disruptive force acts on the bubble to deform it, whereas the restorative force refrains it from deforming.

Dispersed bubble flow pattern is marked by the absence of cap or deformable bubbles, only tiny spherical bubbles remain dispersed in liquid as a homogeneous mixture.

At certain level of liquid turbulence there is a maximum stable diameter of the dispersed phase, d_{max}, which characterizes the dispersion. At this size, bubbles can be deformed, their motion is in a zig-zag path and, if their agglomeration approaches a void fraction value of 0.25, Taylor bubbles can start to appear and transition to slug flow will occur. This size, d_{max}, is determined by the following expression (Hinze, 1955)

$$d_{max} = 0.725 \left(\frac{\sigma}{\rho_L}\right)^{3/5} (\varepsilon)^{-2/5} \tag{1}$$

Where, ε is the rate of energy dissipation per unit mass, and it is defined as follows

$$\varepsilon = \left|\frac{dP}{dz}\right| \frac{V_M}{\rho_M} \tag{2}$$

$\left|\frac{dP}{dz}\right|$ is the frictional pressure loss gradient. For an annulus it is (see **Appendix A**)

$$\left|\frac{dP}{dz}\right| = \frac{2f}{d_h} \rho_M V_M^2 \tag{3}$$

V_M is the mixture velocity

$$V_M = V_{SL} + V_{SG} \tag{4}$$

V_{SL} and V_{SG} are the liquid and gas superficial velocities, respectively.

d_h is the hydraulic diameter

$$d_h = \frac{4 A_c}{P} = d_2 - d_1 \tag{5}$$

d_2 is the inside diameter of the outer pipe and d_1 is the outside diameter of the inner pipe of the annulus, ρ_M is the mixture density and f is the friction factor which depends of the flow behavior index, n, for power-law fluids.

More correlations can be found for the maximum diameter, d_{max}, derived for various flow conditions in a recent extensive study on flow-induced bubble breakup (Jain, 2017).

For modeling of transition criterion an equation explicit in the friction factor is preferred; here, we will use the Blasius-type approximate expression introduced by Irving (1988), equation (A.24), to estimate friction factor under turbulent regime. The one can be organized in a simpler and known form as

$$f = C_f (Re_g)^{-m} \tag{6}$$

where

$$C_f = [F(n)]^{1/(3n+1)} \tag{6a}$$

and

$$m = 1/(3n+1) \tag{6b}$$

$F(n)$ and Re_g are defined in Appendix A, equations (A.25) and (A.15), respectively.

If liquid flow rate is increased at fixed gas flow rate, turbulence forces overcome interfacial tension and gas phase is dispersed into smaller bubbles until they reach a critical size. At this critical size and below, tiny bubbles are spherical and behave as rigid solids, their motion is linear, and they can agglomerate at void fractions bigger than 0.25 without coalescing. An empirical expression to determine this critical bubble size was proposed by Brodkey (1967) as

$$d_{crit} = \left[\frac{0.4\,\sigma}{(\rho_L - \rho_G)\,g}\right]^{1/2} \tag{7}$$

In other words, equation (7) predicts the upper limit at which hydrodynamic bubble behavior is like rigid spheres. But, according to Barnea et al. (1982) bubbles can keep their spherical shape up to about twice the size estimated in Eq. 7. Therefore, equation (7) becomes,

$$d_{crit} = 2\left[\frac{0.4\,\sigma}{(\rho_L - \rho_G)\,g}\right]^{1/2} \tag{8}$$

The bubble/dispersed bubble (BL/DB) transition occurs when $d_{max} = d_{crit}$. If $d_{max} \leq d_{crit}$, bubbles will remain spherical and dispersed bubble flow pattern will prevail. If $d_{max} > d_{crit}$, bubbly flow pattern will exist.

To get the final expression for the transition criterion, we set $d_{max} = d_{crit}$. After substitutions and simplifications, all the above give

$$0.725 = 2\left[\frac{0.4\,\sigma}{g(\rho_L - \rho_G)}\right]^{1/2} \left(\frac{\rho_L}{\sigma}\right)^{3/5} \left[\frac{2\,C_f}{d_h}\left(\frac{d_e^{\,n}\,\rho_L}{K'\,12^{n-1}}\right)^{-m}\right]^{2/5} V_M^{2[3+m(n-2)]/5} \tag{9}$$

K' is defined in equation A.16 for slot flow, and d_e is any equivalent diameter definition which represents the annular.

For a given set of fluid properties and flow geometry data, the transition criterion will reduce to the following type expression

$$V_{SL} = \beta - V_{SG} \tag{9a}$$

where the constant β, is

$$\beta = \left\{ \frac{0.725}{2\left[\frac{0.4\,\sigma}{g(\rho_L-\rho_G)}\right]^{1/2}\left(\frac{\rho_L}{\sigma}\right)^{3/5}\left[\frac{2\,C_f}{d_h}\left(\frac{{d_e}^n\,\rho_L}{K'\,12^{n-1}}\right)^{-m}\right]^{2/5}} \right\}^{5[3+m(n-2)]/2} \tag{9b}$$

From which the boundary of the bubble/dispersed bubble (BL/DB) transition can be drawn on a flow pattern map in terms of superficial velocities.

Dispersed bubble flow pattern will exist even for void fraction bigger than 0.25 when bubbles are at and below their critical size. However, at high gas and liquid superficial velocities, bubbles conglomerate so closely packed and they can reach a certain packing condition where collisions increase suddenly and bubbles will coalesce inevitably to form bigger bubbles, then Taylor bubbles will start to appear and transition to slug flow. The maximum bubble packing has been described by previous authors either by a cubic or a rhombohedral arrangement of spherical bubbles which correspond to approximate void fractions of 0.52 and 0.74, respectively.

From the definition of void fraction and for a cubic bubble arrangement with non-slip condition between phases, we get

$$V_{SL} = 0.923\,V_{SG} \tag{10}$$

This transition criterion is linear, independent of the conduit geometry and ceases BL/DB transition denoted by equation (9). It is shown in figures 2 and 3 as "α = 0.52".

The intermittent / annular (IN/AN) transition

In the vertical upward co-current annular flow a continuous liquid film flows along the wetted wall(s) of the conduit while the gas flows in a central core. Gas core may or may not contain entrained liquid droplets.

The main mechanisms, which govern the flow pattern transition boundary of vertical annular flow regime are described by several authors (Wallis, 1969; Hewitt and Hall-Taylor, 1970; Govier and Azis, 2008; Al-Safran and Brill, 2017). For a set of physical fluids properties, pipe geometrical parameters, and operational conditions, mechanisms interact to define the IN/AN transition.

In this work, the method proposed by Barnea (1986) is modified to account for the non-Newtonian behavior of drilling fluids and the annuli geometry. Barnea (1986) model depends on liquid-film-reversal and film bridging mechanisms and is based on combined momentum balance for gas and liquid phases. The main assumptions of this model are: no entrained droplets in the gas core, uniform liquid-film thickness around gas core, 1D and steady-state flow.

Force balance on liquid film and gas core are given, respectively, as follows:

$$-A_L\frac{dp}{dz} - \tau_L S_L + \tau_I S_I - \rho_L A_L g\sin\theta = 0 \tag{11}$$

$$-A_G\frac{dp}{dz} - \tau_I S_I - \rho_G A_G g\sin\theta = 0 \tag{12}$$

Equating pressure-drop gradients terms in Eqs. 11 and 12 gives the combined momentum equation as,

$$\tau_I S_I\left(\frac{1}{A_L}+\frac{1}{A_G}\right) - \tau_L\frac{S_L}{A_L} - (\rho_L-\rho_G)g\sin\theta = 0 \tag{13}$$

where A_L, A_G, S_L, and S_I are the geometrical relationships, which dependent on the liquid film thickness. In terms of equivalent diameter of the annuli, d_e, and dimensionless liquid film thickness, δ/de, they are

$$S_L = \pi d_e \tag{14}$$

$$S_I = \pi\,d_e\left(1-2\tilde{\delta}\right) \tag{15}$$

$$A_L = \pi\,{d_e}^2\left(\tilde{\delta}-\tilde{\delta}^2\right) \tag{16}$$

$$A_G = \frac{\pi\,{d_e}^2}{4}\left(1-2\tilde{\delta}\right)^2 \tag{17}$$

Liquid shear stress at pipe wall in Eq. 13, τ_L, is given as

$$\tau_L = f_L\frac{\rho_L V_L^2}{2} \tag{18}$$

The liquid friction factor is defined by a Blasius-type equation as,

$$f_L = C_f\left(Re_g\right)^{-m} \tag{19}$$

However, in annular flow, liquid phase flows through a thin ring between the periphery of the gas core and the wall(s) of the conduit. Thus, to determine the characteristic length required to define the generalized Reynolds number in equation (19) we will use the hydraulic diameter, calculated as

$$d_h = \frac{4\,A_L}{S_L} = \delta - \frac{\delta^2}{d_e} = 4\,d_e\left(\tilde{\delta}-\tilde{\delta}^2\right) \tag{20}$$

And actual liquid velocity in terms of $\tilde{\delta}$ is defined as follows

$$V_L = \frac{q_L}{A_G} = \frac{V_{SL}}{4\left(\tilde{\delta}-\tilde{\delta}^2\right)} \tag{21}$$

Substitution of Eqs. 20 and 21 into equation (A.15) gives

$$\mathrm{Re_g} = \frac{d_e^{n}\ \rho_L\ {V_{SL}}^{2-n}\ [4(\tilde{\delta}-\tilde{\delta}^2)]^{(2n-2)}}{K'\ 12^{n-1}} \tag{22}$$

Coefficients in Eq. 19 are: $C_f = 24$ and $m = 1$ for a laminar liquid film and C_f and m as defined previously in equations (6a) and (6b) for a turbulent flow in the film. The critical value of Re_g at the laminar-to-turbulent transition from the Ryan and Johnson (1959) criterion, see Eq. A.26, with Re_g of the liquid film defined by Eq. 22.

After solving the combined momentum equation for the interfacial shear stress, substituting geometrical relationships in terms of the dimensionless average film thickness, and re-arranging, we obtain

$$\tau_I = g\,(\rho_L - \rho_G)\,d_e\,\mathrm{Sin}\,\theta\,\left(\tilde{\delta} - \tilde{\delta}^2\right)\left(1-2\tilde{\delta}\right) + \frac{C_L\,\rho_L}{32}\left(\frac{{d_e}^{n}\ \rho_L}{12^{n-1}\ K'}\right)^{-m}\frac{{V_{SL}}^{2+m(n-2)}}{4^{m(2n-2)}}\left[\frac{(1-2\tilde{\delta})}{\left(\tilde{\delta}-\tilde{\delta}^2\right)^{2+m(2n-2)}}\right] \tag{23}$$

The previous equation can be reduced to this type

$$\tau_I = (\beta 1)\ \left(\tilde{\delta} - \tilde{\delta}^2\right)\left(1-2\tilde{\delta}\right) + (\beta 2)\left[\frac{\left(1-2\tilde{\delta}\right)}{\left(\tilde{\delta}-\tilde{\delta}^2\right)^{\beta 3}}\right] \tag{23a}$$

where β1, β2, and β3 are constants for a given set of data.

The relation between interfacial shear stress, τ_I, and the dimensionless average film thickness, $\tilde{\delta}$, is illustrated on previous equation. Graphical illustrations of $\tilde{\tau}_I$ versus $\tilde{\delta}$ are shown in Figs. 4 to 12 with the dimensionless interfacial shear stress defined as follows

$$\tilde{\tau}_I = \tau_I / g\,(\rho_L - \rho_G)\,d_e \tag{24}$$

Solids curves in Figs. 4 to 7 are for several values of V_{SL}. In figure 4 the Newtonian case and figure 5 to 7 with different n-values, the additional data of fluids properties and annulus geometry is listed in Table 1. Plotting $\tilde{\tau}_I$ as a function of $\tilde{\delta}$ at different parametric values of liquid superficial velocity shows how interfacial shear stresses changes with changing the superficial liquid velocity. The minimum value depicted in Figs. 4 to 7 represents a flow direction change, indicating reversal flow of the liquid film. The left side of this minimum corresponds to stable solutions in positive upward flow direction, while the right side of this minimum corresponds to unstable solutions with negative liquid film velocity, i.e. flow in downward direction.

To find this critical thickness value we can use the concept of the derivate, which enables us to find minimum and maximum values.

Differentiating Eq. 23 with respect to $\tilde{\delta}$, we obtain,

$$g\,(\rho_L - \rho_G)\,d_e\,\mathrm{Sin}\,\theta\,\left(1 - 6\tilde{\delta} + 6\tilde{\delta}^2\right) + \frac{C_L\rho_L}{32}\left(\frac{{d_e}^{n}\ \rho_L}{12^{n-1}K'}\right)^{-m}\frac{{V_{SL}}^{2+m(n-2)}}{4^{m(2n-2)}}\left\{\frac{[m(2-2n)-2]\left(1-2\tilde{\delta}\right)^2 - 2\left(\tilde{\delta}-\tilde{\delta}^2\right)}{\left(\tilde{\delta}-\tilde{\delta}^2\right)^{3+m(2n-2)}}\right\} = 0 \tag{25}$$

Eq. 25 give the critical minimum value of the liquid thickness. In Figs. 8 to 11 we added the solutions for the V_{SG} by using the Wallis (1969) expression for the interfacial shear stress in terms of $\tilde{\delta}$.

$$\tau_I = \frac{1}{2} f_I\,\rho_G\,\frac{{V_{SG}}^2}{\left(1-2\tilde{\delta}\right)^4} \tag{26}$$

Eq. 26 provides the relation between interfacial shear stress and gas flow rate, where

$$f_I = f_G\left(1 + 300\,\tilde{\delta}\right) \tag{27}$$

and

$$f_G = C_G\left(\frac{d_e\,\rho_G\,V_{SG}}{\mu_G}\right)^{-m} \tag{28}$$

Eq. 27 is an empirical relationship for f_I with gas friction factor, f_G, determined as if only gas phase were flowing inside of the conduit. Coefficients in Eq. 28 are: $C_G = 0.046$ and $m = 0.2$ for turbulent flow regime, and $C_G = 16$ and $m = 1$ for laminar flow regime.

The intersection of V_{SL} and V_{SG} values at the minimum point represents the IN/AN transition, the stable solution, which it is related to critical film thickness value. The points of the IN/AN transition by film stability mechanism are obtained by solving simultaneously Eq. 23 and 26 with a dimensionless liquid film thickness value, $\tilde{\delta}$, which satisfices Eq. 25, i.e. its minimum value.

However, as mentioned in Barnea (1986), the mechanism of blockage of the gas core also acts in this transition criterion. The blockage of the gas core occurs at higher gas flow rates when liquid waves (formed due to high liquid supply) can connect and block the conduit, therefore initiating the transition to intermittent flow pattern regime (slug/churn). They considered that intermittent flow will occur when

$$\frac{A_L}{A} = 0.5\ R_{sm} \tag{29}$$

R_{sm} is the minimal liquid holdup of the liquid bridge, which will create blockage of the gas passage and it is related to the liquid holdup in a maximum bubble packing arrangement. If a bubble cubic packing in slug body is considered, liquid holdup is approximately 0.48 which corresponds to $\tilde{\delta} = 0.064$. Consequently, Eq. 29 becomes:

$$\frac{A_L}{A} = (0.5\,)(0.48) = 0.24 \tag{30}$$

Then to construct the curve for the IN/AN transition on a flow pattern map in terms of superficial velocities, we need to consider both mechanisms as follows:

1. Simultaneously solve Eq. 23 and 26 with a dimensionless liquid film thickness value, $\tilde{\delta}$, which satisfices Eq. 25.
2. If $\tilde{\delta}$ determined in the latter step is smaller than the value indicated by Eq. 29, i.e. $\tilde{\delta} = 0.064$; then, the transition to intermittent flow will occur due to film stability mechanism.
3. If $\tilde{\delta}$ determined in step 1 is greater than the value of 0.064 then, the transition to intermittent flow will occur due to the blockage of the gas core at $\tilde{\delta} = 0.064$.

Note that the occurrence of the mechanism of blockage of the gas core requires high liquid flow rates at high gas flow velocities. In other words, the transition to intermittent flow from annular flow owing to film instability would occur at low liquid flow rates, and the same transition due to blockage of the gas core occurs at high liquid flow rates, with high gas flow rate in both situations.

A more extensive explanation and discussion of both mechanisms of transition from annular flow to intermittent flow pattern regime have been carried out in Barnea (1986).

Results and discussions

Results of this study reveal the flow pattern prediction due to the inclusion of the power-law non-Newtonian model and the annular geometry into existing models. Note that the modified models reduce to the original model when n = 1 and $d_e = d_h = d$. The simulated results shown below were developed using the dataset provided in Table 1.

The bubble/dispersed bubble (BL/DB) transition. If we chose the hydraulic diameter as the equivalent diameter for the annulus representation, i.e. $d_e = d_h$. Eq. 9 becomes

$$0.725 = 2\left[\frac{0.4\,\sigma}{g(\rho_L-\rho_G)}\right]^{1/2}\left(\frac{\rho_L}{\sigma}\right)^{3/5}\left[\frac{2\,C_f}{d_h^{\,1+mn}}\left(\frac{\rho_L}{K'\,12^{n-1}}\right)^{-m}\right]^{2/5} V_M^{2[3+m(n-2)]/5} \quad (9c)$$

Note that d_e can be any equivalent or effective diameter definition (see Table A.1). This BL/DB transition boundary is plotted in Figs. 2 and 3 for the given set of synthetic data displayed in Table 1. The continuous black curve represents the Newtonian case (n =1), and dashed-curves represent the non-Newtonian scenarios (n = 0.8, n = 0.6, and n = 0.4, all with the same K). The end of the BL/DB transition when dispersed bubbles reach the physical limit of the maximum bubble packing and transition to slug flow happens (even at high turbulence levels), is shown by the continuous black line with markers, denoted as "α = 0.52" on plots and computed from Eq. 10. Note on both figures that when non-Newtonian behavior increases, i.e. when $n \to 0$, higher liquid flow rates are needed to reach the transition BL/DB. It can be explained theoretically by means of the shear thinning behavior of the pseudo-plastic liquids, their "apparent or effective viscosity" reduces when shear rate increases. This reduction in "apparent viscosity" is greater at smaller n-values and reduces turbulence in liquid phase, which increases bubble diameter, i.e. expanding bubble flow region. Consequently, more liquid flow rate is required at the mixture for smaller n-values to increase turbulence and reach the required energy of dissipation for the BL/DB transition occurrence.

The annular geometry has different effect on the transition. In Fig. 2, a *6.625 X 3.5-in* annulus with a diameter ratio, κ, equal to 0.528 was used. In figure 3, a *4 X 2.11-in* annulus with the same κ (0.528) was taken. Note that even both annuli have the same κ, the transition BL/DB differs. The transition occurs at smaller liquid flow rates for the case of the annulus with smaller clearance, defined as the distant between the two walls of the concentric annulus $[(d_2 - d_1)/2]$. For a constant flow rate, high levels of turbulence are reached in smaller gaps due to higher friction factor. A quick look of the Blasius-type friction factor formula and the Reynolds number definition illustrates this fact by using the annular clearance as the characteristic length.

The intermittent/annular (IN/AN) transition.

In Figs. 4 to 12, the relation between $\tilde{\tau}_I$ and $\tilde{\delta}$ for vertical upward flow of a gas and power-law fluid mixture through concentric annuli for different n-values at different superficial-liquid-velocity values are shown as solid curves. The solid curves display a minimum value, which represents a change in superficial liquid velocity, indicating a flow direction change in the liquid film, i.e. film reversal. The locus of these minimum values is depicted in Figs. 4, 9, 11, and 12 by a thick blue solid line, which cuts transversally steady-state solutions for several V_{SL} at their minimum. This minimum value is linked to a critical film thickness and it is found from Eq. (25).

A look at Figs. 4 to 7 (different n-values) we can state that critical liquid film thickness becomes thinner at smaller n-values. In other words, when non-Newtonian behavior increases, equilibrium of the liquid film is reached at lower interfacial shear stresses (or superficial-gas-velocity).

Once the minimum value of interfacial shear stress is determined, the critical gas velocity is obtained from Eq. (26). Solutions of τ_I for several superficial-gas-velocities are plotted in Figs. 8 to 11 like dashed lines; values of n changes in each plot. The intersection of the broken and solid curves yields the steady-state solution.

In Fig. 9, the thick blue solid line links the locus of minimum values of liquid film thickness. According to the film stability mechanism or criterion, the branch of steady-state solutions to the left of the thick blue solid line corresponds to stable steady-state solutions with a positive velocity profile; one of these solutions is represented by the black triangle on figure 9. On the other hand, the right-hand branch of solutions corresponds to unstable steady-state solutions with a negative profile close to the conduit wall(s), one of these solutions is

represented by the black circle in the same Fig.

The second mechanism of IN/AN transition is the blockage of the gas core, which is depicted as a vertical red line (at $\tilde{\delta} = 0.064$) in Figs. 8 to 11. Solutions from this second mechanism are represented as black diamonds (markers) on Fig. 9 for V_{SL} = 1.5 m/s and V_{SL} = 2.5 m/s at n = 0.8, while on Fig. 10 they are the solutions for V_{SL} = 2.5 m/s and V_{SL} =5 m/s at n = 0.6.

From observation of Figs. 8 to 11, one can conclude that the IN/AN transition is more dominated by the film-stability mechanism when the non-Newtonian behavior increases (smaller n-values). The transition to intermittent flow due to the second mechanism requires higher liquid flow rates, which are difficult to reach in drilling operations.

Fig. 12 is for a smaller annular gap (a *4 X 2.11-in* annulus) with the same rest of the data (n = 0.4) used in Fig. 11 (see table 1). From visual inspection of Figs. 11 and 12, one can observe that steady-state solutions (linked by the thick blue solid line on both figures) arise at lower interfacial shear stress and lower dimensionless film thickness for the wider annular gap. A narrower annular gap promotes liquid film bridging and blockage of the gas core, while high liquid velocities are still important parameter.

The IN/AN transition curves for different n-values are plotted on a flow pattern map in Fig. 13. For comparison, we also plotted the Taitel et al. (1980) transition criterion, which corresponds to the minimum gas velocity required to suspend a liquid droplet. The IN/AN transition predicted by the developed model occurs at gas-superficial velocities for all n-values at a higher transition estimated by the Taitel et al. (1980) criterion.

As can be seen, at low liquid flow rates the liquid-film stability dominates the IN/AN transition. For the given set of data, curves for all n-values practically collapse for liquid flow rates lower than 1 m/s, above which the film bridging mechanism becomes more important into the IN/AN transition.

Transitions for two different annular geometries are shown in Fig. 14. Both cases have the same fluid properties (n = 0.8) and diameter ratio (κ = 0.528), with the only difference being the clearance of the annulus. As mentioned above, when the annular gap reduces the transition to intermittent flow is promoted due to the film bridging. The IN/AN transition due the blockage of the gas core begins at about V_{SL} = 0.9 m/s for the *6.625 X 3.5-in* annulus, while for the narrower annulus (*4 X 2.11-in*) it begins around V_{SL} = 0.6 m/s.

Summary

The following concluding remarks are derived from this work:

1. Two new transition models were theoretically developed to account for the shear thinning effect of pseudo-plastic fluids and the annular geometry in terms of equivalent diameter definitions. The DB/BL transition was derived from the original model presented by Taitel et al. (1980) and the IN/AN transition from the model originally proposed by Barnea (1986).
2. The key differences between the modified and original models are the incorporation of (a) the generalized Reynolds number for a power-law fluid taken from the annulus representation as an slot, (b) a Blasius-type friction factor correlation for power-law fluids, (c) a laminar-to-turbulent transition criteria for power-law fluids, and (d) equivalent diameter to treat the annulus as a pipe, into both transition models.
3. In this theoretical work, we considered the hydraulic diameter as equivalent diameter to mimic the annulus, but any other equivalent or effective diameter definition can be used. More definitions are listed in Table A.1.
4. The shear-thinning behavior of the liquid phase has a greater effect on the transition boundary of BL/DB than on the IN/AN transition limit. This agrees with the fact that liquid-phase prevails as continuous phase along BL/DB transition, which occurs at high liquid superficial velocities while in the IN/AN transition the gas void fraction increases considerably. In addition, no liquid entrainment fraction in the IN/AN flow pattern transition model was considered.
5. When non-Newtonian behavior increases, i.e. $n \rightarrow 0$, higher liquid velocities are required to reach a critical level of turbulence and energy dissipation to break large bubble into small ones and transition to dispersed bubble flow.
6. As annular gap decreases, a transition to dispersed is promoted at lower liquid velocities.
7. Steady-state solutions in annular flow pattern occur at thinner liquid-film thicknesses and lower interfacial-shear stresses when non-Newtonian behavior increases.
8. For the used data set in this study, IN/AN transition is dominated by the film stability mechanism. Transition boundaries for all n-values overlap for liquid velocities lower than 1 m/s, above which the film bridging mechanism becomes more important into the transition.
9. When the annular gap decreases the IN/AN transition occurs due to the film bridging mechanism domination at lower liquid velocities.
10. In general, shear thinning is probably the most significant rheological effect that reduces both film thickness and friction when a gas and pseudo-plastic liquid mixtures flow inside of circular closed conduits.

Acknowledgments

This research work was stablished by the Production and Drilling Research Project (PDRP) at New Mexico Institute of Mining and Technology and the National Council of Science and Technology (CONACYT) of Mexico.

Nomenclature

K = Consistency index, $Pa.s^n$
n= Flow behavior index, dimensionless
g= Gravity acceleration constant = 9.81 m/s^2
Re_g = Generalized Reynolds number, dimensionless
V_M=Mean or mixture velocity, m/s
V_{SL} = Liquid superficial velocity, m/s
V_{SG} = Gas superficial velocity, m/s
A = Area, m^2
S = Perimeter, m
V = Actual velocity, m/s
f = Fanning friction factor, dimensionless
q = Volumetric flow rate, m^3/s
g_c = conversion factor
m = meter
s = second
N = Newton
Pa = Pascal

Greek letters:

σ = Liquid surface tension, N/m
μ = Viscosity, Pa.s
θ = Inclination angle, radians
τ = Shear stress, Pa
π = Constant $\approx$ 3.1416
κ = Diameter ratio, dimensionless
α = Void fraction, dimensionless
ρ = density, Kg/m^3

Subscripts:

L = Liquid
G = Gas
1 = i = Inner
2 = o = Outer
I = Interfacial
w = Wall
avg = Average
M = Mixture

Table 1. Input data used to build transition curves.

	Figure 2	Figure 3	Figures 4-11 and 13	Figures 12 and 14
ID Casing, in	6.625	4	6.625	4
OD Drillstring, in	3.5	2.113	3.5	2.113
Liquid Density, Kg/m^3	1050	1050	1050	1050
Gas Density, Kg/m^3	1.225	1.225	1.2	1.2
Gas Viscosity, Kg/(m.s)	0.0002	0.0002	0.0002	0.0002
Superficial tension, N/m	0.073	0.073	0.073	0.073
Consistency Index, K, ($Pa\ s^n$)	0.005	0.005	0.003	0.003
Diameter Ratio, dimensionless	0.528	0.528	0.528	0.528
Hydraulic Diameter, m	0.0793	0.0479	0.0793	0.0479
Inclination Angle, degrees	90	90	90	90
Equivalent diameter	d_h	d_h	d_h	d_h

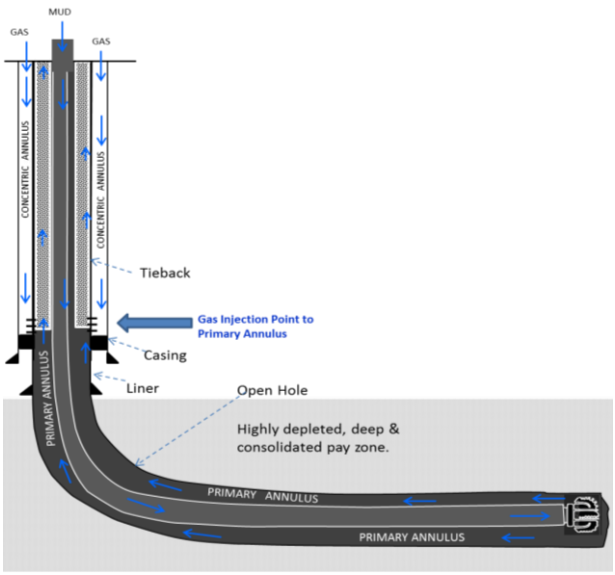

Figure 1. Schematic of CCGI system. When drilling only liquid mud is going inside the drill pipe and multiphase flow occurs along the primary annulus.

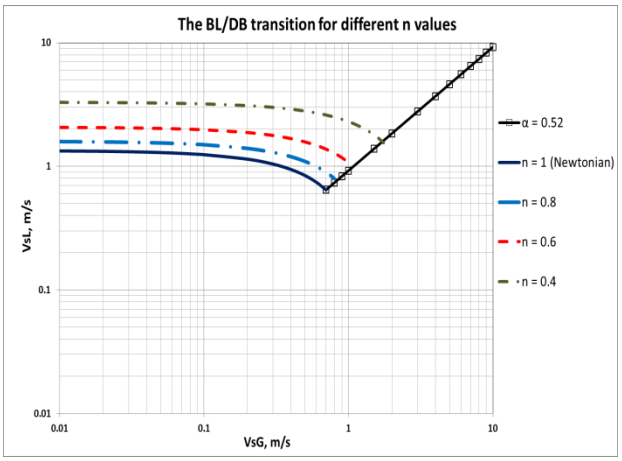

Figure 2. Effect of fluid rheology on DB/BL transitions boundary of an air-pseudoplastic liquid mixture (with κ=0.528, 90°, and d_h=0.079 m).

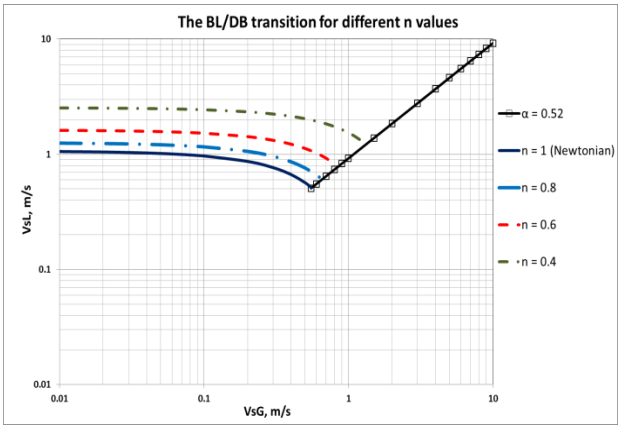

Figure 3. Effect of fluid rheology on DB/BL transitions boundary of an air-pseudoplastic liquid mixture (with κ=0.528, 90°, and d_h=0.047 m).

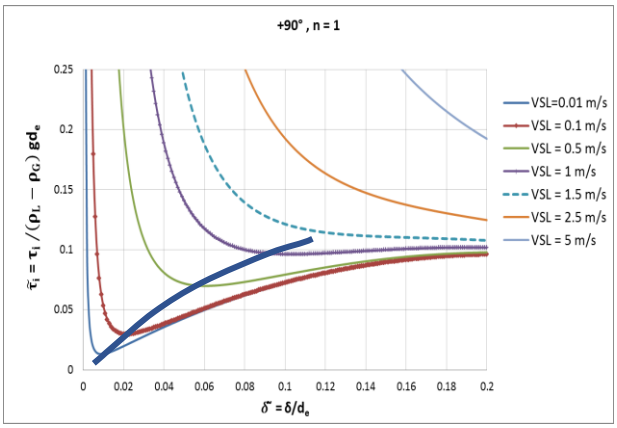

Figure 4. Relationship of dimensionless interfacial shear stress and dimensionless film thickness at several liquid superficial velocities in a *6.625 X 3.5-in* annulus. Newtonian case.

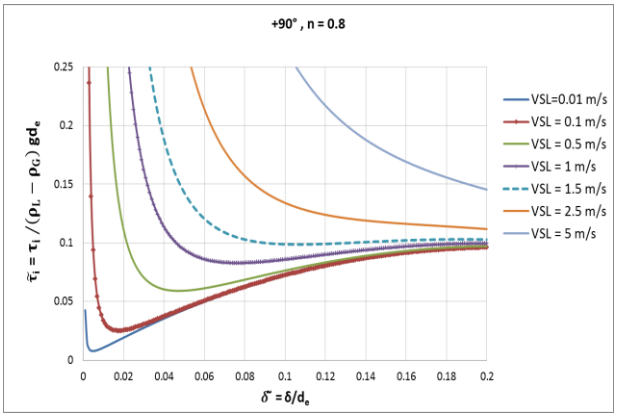

Figure 5. Relationship of dimensionless interfacial shear stress and dimensionless film thickness at several liquid superficial velocities in a *6.625 X 3.5-in* annulus with n = 0.8

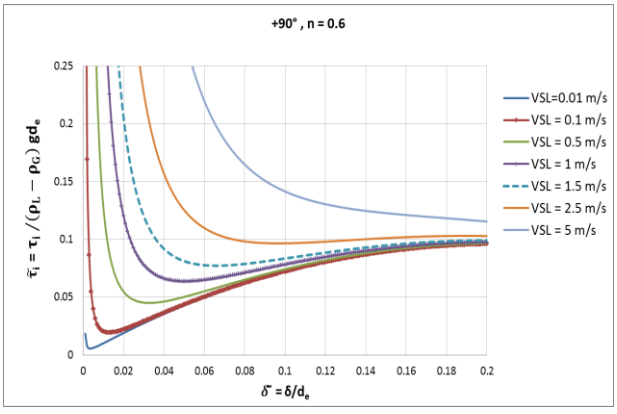

Figure 6. Relationship of dimensionless interfacial shear stress and dimensionless film thickness at several liquid superficial velocities in a *6.625 X 3.5-in* annulus with n = 0.6.

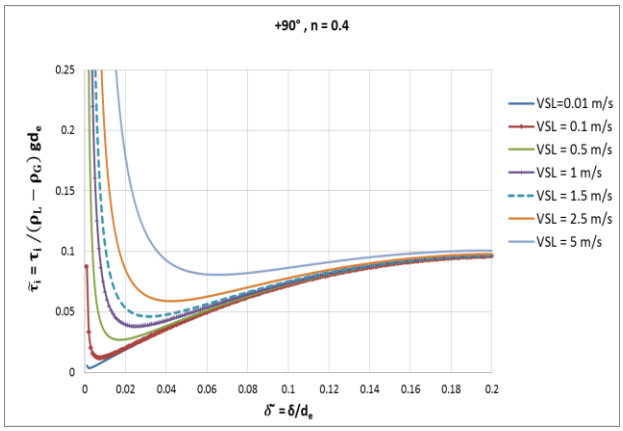

Figure 7. Relationship of dimensionless interfacial shear stress and dimensionless film thickness at several liquid superficial velocities in a *6.625 X 3.5-in* annulus with n = 0.4.

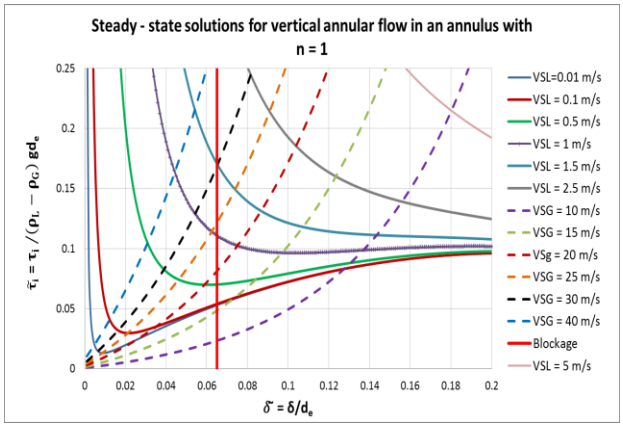

Figure 8. Relation of dimensionless interfacial shear stress and dimensionless film thickness at several liquid and gas superficial velocities in a *6.625 X 3.5-in* annulus with n = 1.

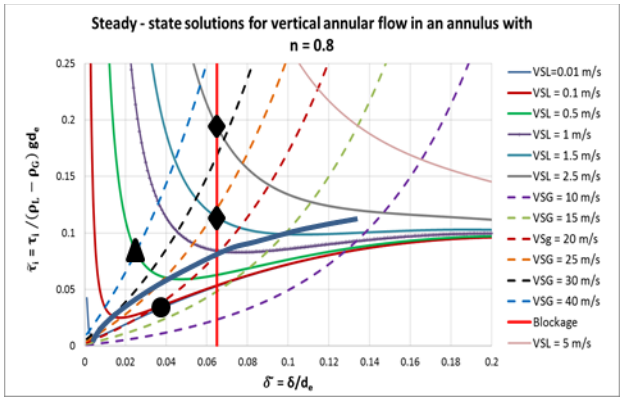

Figure 9. Relationship of dimensionless interfacial shear stress and dimensionless film thickness at several liquid and gas superficial velocities in a *6.625 X 3.5-in* annulus with n = 0.8.

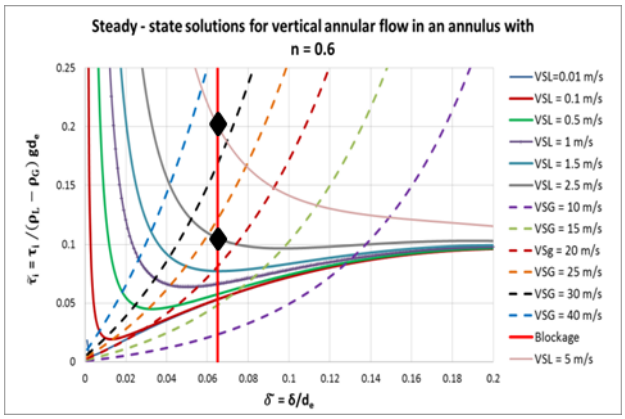

Figure 10. Relationship of dimensionless interfacial shear stress and dimensionless film thickness at several liquid and gas superficial velocities in a *6.625 X 3.5-in* annulus with n = 0.6.

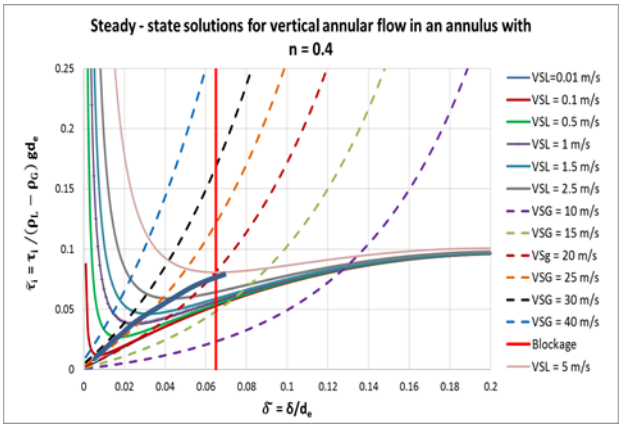

Figure 11. Relation of dimensionless interfacial shear stress and dimensionless film thickness at several liquid and gas superficial velocities in a *6.625 X 3.5-in* annulus with n = 0.4.

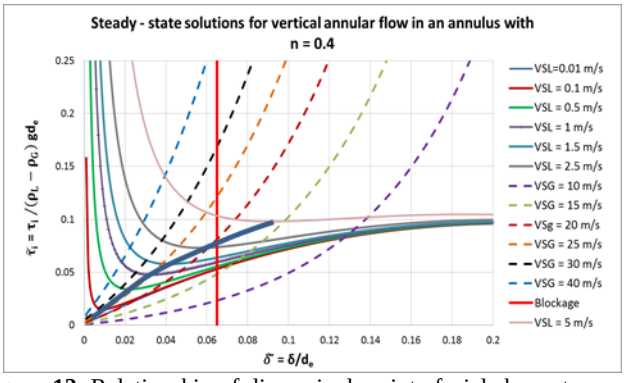

Figure 12. Relationship of dimensionless interfacial shear stress and dimensionless film thickness at several liquid and gas superficial velocities in a *4 X 2.11-in* annulus with n = 0.4.

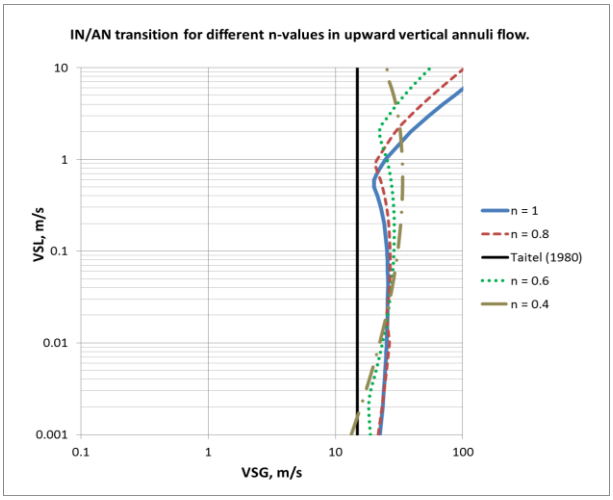

Figure 13. Effect of fluid rheology on IN/AN transition boundary for an air-pseudoplastic liquid mixture (κ=0.528, 90°, and d_h=0.079 m).

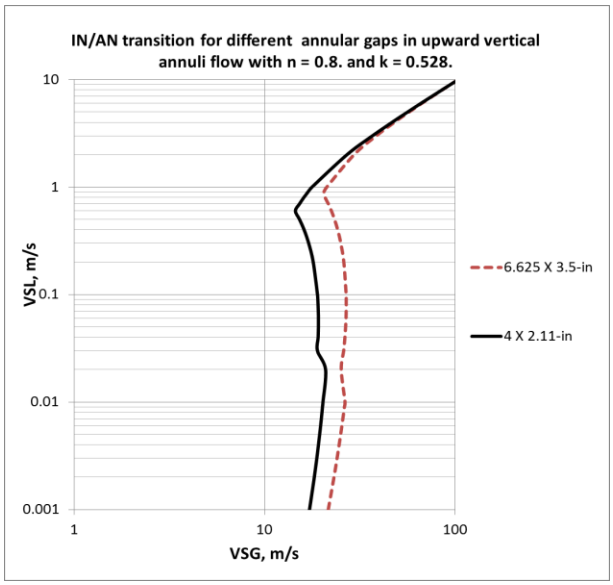

Figure 14. Effect of annular gap on IN/AN transition boundary for an air-pseudoplastic liquid mixture (κ=0.528, 90°, and n=0.8).

References

1. Al-Safran, E. M., and Brill, J. P. (2017). Applied Multiphase Flow in Pipes and Flow Assurance (1st ed.). Richardson, TX, USA: SPE Textbook Series.
2. Barnea, D. (1986). Transition From Annular Flow and From Dispersed Bubble Flow: Unified Models for the Whole Range of Pipe Inclinations. *Int. J. Multiphase Flow*, **12** (5), 733-744.
3. Barnea, D., and Shemer, L. (1986). Rise Velocity of Large Bubbles in Stagnant Liquid in Non-Circular Ducts. *Int. J. Multiphase Flow*, **12** (6), 1025-1027.
4. Barnea, D., Shoham, O., and Taitel, Y. (1982). Flow Pattern Transition for Vertical Downward Two-Phase Flow. *Chem. Eng. Sci*., **37** (5), 741-744.
5. Beltran, J. C., Lupo, C., Medina, L., Duno, H., Gallo, F., Tang, J., and Puerto, G. (2010). Understanding Multiphase Flow Modeling for N2 Concentric Nitrogen Injection through Downhole Pressure Sensor Data Measurements While Drilling MPD Wells. Paper presented at the 2010 SPE/IADC Managed Pressure Drilling and Underbalanced Operations Conference and Exhibition held in Kuala Lumpur, Malaysia, 24-25 February 2010. SPE/IADC 130324-MS.
6. Bird, R., E, S. W., and Lightfoot, E. N. (1976). Transport Phenomena. New York, USA: John Wiley.
7. Bourgoyne Jr., A., Millheim, K., Chenevert, M., and Young, F. (1986). Applied Drilling Engineering. Richardson, TX, USA: SPE of AIME.
8. Brodkey, R. S. (1967). The Phenomena of Fluid Motion. New York: Addison-Wesley Press.
9. Crittendon, B. (1959). The Mechanics of Design and Interpretation of Hydraulic Fracture Treatments. Paper presented at 33rd Annual Fall Meeting of the Society of Petroleum Engineers at Houston, Tex. Oct. 5-8, 1958. SPE 1106-G and JPT, 21-29.
10. David, J., and Filip, P. (1995). Relationship of Annular and Parallel-Plate Poiseuille Flows for Power-Law Fluids. *Polym.-Plast. Technol. Eng.*, **34**(6), 947-960.
11. Dodge, D., and Metzner, A. (1959). Turbulent Flow of Non-Newtonian Systems. *AIChE J*., **5**(2), 189-204.
12. Dosunmu, I., and Shah, S. (2015). Friction Pressure Prediction for Annular Flow of Power Law Fluids. *Chemical Engineering Communications*, **202**, 1380-1388.
13. Frederick, A., and Bird, R. (1958). Non-Newtonian Flow in Annuli. *Ind. Eng. Chem.*, **50**(3), 347-352.
14. Govier, G., and Aziz, K. (2008). The Flow of Complex Mixtures in Pipes (Second ed.). Richardson, TX, USA: SPE.
15. Guillot, D., and Denis, J. (1988). Prediction of Laminar and Turbulent Friction Pressures of Cement Slurries in Pipes and Centered Annuli. Paper prepared for presentation at the SPE European Petroleum Conference, London, UK October 16-19, 1988. SPE 18377-MS, 379-388.
16. Hewitt, G., and Hall-Taylor, N. (1970). Annular Two-Phase Flow (First Edition ed.). New York, USA: Pergamon Press.
17. Hinze, J. O. (1955, Sep). Fundamentals of the Hydrodynamic Mechanism of Splitting in Dispersion Processes. *AIChE J*., **1**(3), 289-295.
18. Irvine, T. F. (1988). A generalized Blasius Equation for Power Law Fluids. *Chem. Eng. Comm.*, **65**, 39-47.
19. Jain, S. S. (2017, Jan). Flow-Induced Breakup of Drops and Bubbles. Elsevier, 1-56.
20. Jensen, T., and Sharma, M. (1987, Dec). Study of Friction Factor and Equivalent Diameter Correlations for Annular Flow of Non-Newtonian Drilling Fluids. *ASME Trans.*, **109**, 200-205.
21. Jones, O. C. (1976, Jun). An Improvement in the Calculation of Turbulent Friction in Rectangular Ducts. *Journal of Fluids Engineering, ASME Trans.*, 173-180.
22. Jones, O. J., and Leung, J. (1981). An Improvement in the Calculation of Turbulent Friction in Smooth Concentric Annuli. *Journal of Fluid Engineering*, **103**, 615-623.
23. Knudsen, J., and Katz, D. (1958).Fluid Dynamics and Heat Transfer. USA: McGraw-Hill Series in Chemical Engineering.
24. Lamb, H. (1945). Hydrodynamics (6th ed.). New York City: Dover Publications.
25. Lohrenz, J., and Kurata, F. (1960). A Friction Factor Plot for Smooth Circular Conduits, Concentric Annuli, and Parallel Plates. *Ind. Eng. Chem.*, **52**, 703-706.
26. Meter, D., and Bird, R. (1961, Mar). Turbulent Newtonian Flow in Annuli. *AIChE J*., **7**(1), 41-45.
27. Metzner, A., and Reed, J. (1955, Dec). Flow of Non-Newtonian Fluids-Correlation of the Laminar, Transition, and Turbulent-flow Regions. *AIChE. J.*, **1**(4), 434-440.

28. Mykytiw, C. G., Davidson, I. A., and Frink, P. (2003). Design and Operational Considerations to Maintain Underbalanced Conditions with Concentric Casing Injection. Paper prepared for presentation at the IADC/SPE Underbalanced Technology Conference and Exhibition held in Houston, Texas, USA, 25-25 March 2003. IADC/SPE 81631-MS.
29. Perez, C., Urbieta, A., Lupo, C., Castellanos, J., Ramirez, O., Puerto, G., and Bedoya, J. (February, 2009). First Application of Concentric Nitrogen Injection Technique for a Managed Pressure Drilling Well in Southern Mexico. Paper prepared for presentation at the IADC/SPE Managed Pressure Drilling and Underbalanced Operations Conference and Exhibition held in San Antonio, Texas, USA, 12-13 February 2009. IADC/SPE 122198-MS.
30. Pérez-T., C., Urbieta, A., Lupo, C., Castellanos, J. M., Ramirez, O., Puerto, G., Castiblanco, G. (2009). MPD Concentric Nitrogen Injection Used to Drill a Successful Horizontal Well in Fractured and depleted Mature Reservoir in Mexico South Region. Paper prepared for presentation at the SPE Latin American and Caribbean Petroleum Engineering Conference held in Cartagena, Colombia, 31 May-3 June 2009. SPE 122982-MS.
31. Pilehvari, A., and Serth, R. (2009, Dec). Generalized Hydraulic Calculation Method for Axial Flow of Non-Newtonian Fluids in Eccentric Annuli. *SPE Drill. Complet.* **24**(4), 553-563. SPE 111514-PA
32. Reed, T., and Pilehvari, A. (1993). A New Model for Laminar, Transitional and Turbulent Flow of Drilling Muds. Paper presented at the SPE Production Operations Symposium, Oklahoma City, Oklahoma, USA, 21-23 March 1993. SPE 25456-MS.
33. Rodriguez, R., Franco, R., Gamez, G., Blas, B., Gonzalez, F., Vasquez, J. L., and Alcudia, H. (2013). Successful Application of Concentric Casing Nitrogen Injection to Overcome Drilling Challenges and Deliver a Record Horizontal Well in the Tecominoacan Field. Paper prepared for presentation at the SPE/IADC Drilling Conference and Exhibition held in Amsterdam, The Netherlands, 5-7 March 2013. SPE/IADC 163494-MS.
34. Ryan, N., and Johnson, M. (1959, Dec). Transition from Laminar to Turbulent Flow in Pipes. *AIChE J.*, **5**(4), 433-435.
35. Sadatomi, M., Sato, Y., and Saruwatari, S. (1982). Two-Phase Flow in Vertical Noncircular Channels. *Int. J. Multiphase Flow*, **8**(6), 641-655.
36. Scheid, C., Calcada, L., Rocha, D., Aranha, P., Aragao, A., and Martins, A. (2009). Prediction of pressure losses in drilling fluid flows in circular and annular pipes and accesories. Paper prepared for presentation at the SPE Latin American and Caribbean Petroleum Engineering Conference held in Cartagena, Colombia, 31 May-3 June 2009. SPE 122072-MS.
37. Taitel, Y., Barnea, D., and Duckler, A. (1980, May). Modeling Flow Pattern Transitions for Steady Upward Gas-Liquid Flow in Vertical Tubes. *AIChE J.*, **26**(3), 345-354.
38. Urbieta, A., Lupo, C., Castellanos, J., Scarcelli, D., Ramirez, O., Puerto, G., and Bedoya, J. (2009). First Application in Mexico and New World Depth Record for MPD Concentric Nitrogen Injection to Drill Horizontal Wells in Low Pressure Reservoirs at Samaria Field. Paper prepared for presentation at the SPE/IADC Drilling Conference and Exhibition held in Amsterdam, The Netherlands, 17-19 March 2009. SPE/IADC 119912-MS.
39. Wallis, G. (1969). One-dimensional Two-phase Flow. New York: McGraw Hill.

Appendix A

Unweighted drilling fluids which contain clay or polymer in their formulation, with low or no yield stress, behaves usually as pseudo-plastic fluids. Pseudo-plastic fluids are classified as time-independent non-Newtonian fluids (sometimes denoted to as "non-Newtonian viscous fluids" or alternatively like "purely viscous fluids").

Pseudo-plastic fluids can be rheologically characterized by the power-law or Ostwald-deWaele model. The constitutive equation is

$$\tau_{yx} = \frac{K}{g_c}\left(\frac{du}{dy}\right)^n = \frac{K}{g_c}\left|\frac{du}{dy}\right|^{n-1}\frac{du}{dy} \quad (A.1)$$

By analogy with Newtonian fluids an "apparent or effective viscosity" for pseudo-plastic fluids is defined as

$$\mu_a = \frac{\tau_{yx}\, g_c}{du/dy} = K\left|\frac{du}{dy}\right|^{n-1} = \frac{K}{|du/dy|^{1-n}} \quad (A.2)$$

Since for pseudo-plastic fluids, n < 1, evaluation of equation (A.2) shows that the apparent viscosity decreases with increasing shear rate, this is known as shear thinning behavior and it is sometimes considered synonymous for pseudo-plastic behavior. Note that shear thinning effect increases as behavior index, n, decreases.

Fanning friction factor, f, can be defined as a proportionally constant between wall stress and kinetic energy per unit volume in terms of average velocity as

$$\tau_w = f\ \frac{1}{2}\ \rho\ v_{avg}^2 \quad (A.3)$$

From a force balance of the applied force causing the flow and the shear force arising at the boundary of the conduit to equilibrate the system in steady flow of a fluid in a horizontal position of cross section, Ac, wetted perimeter, P, and length, L, we obtain

$$\tau\, LP = \Delta p\, A_c \quad (A.4)$$

Note that shear stress counterbalances pressure driving force and it acts in a direction opposite the flow direction.

If we applied to the whole cross section and because flow is steady, i.e. the sum of these two forces is zero, wall shear stress or wall stress is

$$\tau_w = \left(\frac{\Delta p}{L}\right)\left(\frac{A_c}{P}\right) \quad (A.5)$$

Parallel plates and pipes share the fact that for a given cross section the wall stress is constant along the perimeter. But in annuli, the wall stress is not constant along the perimeter. Its magnitude is not the same at the inner and outer walls of the annulus, i.e. $\tau_{w\,inner\,wall} \neq \tau_{w\,outer\,wall}$. That is why some authors have defined an average wall stress for the annulus case, e.g. Reed and Pilehvari (1993).

$$\tau_{w\,avg} = (\tau_2 d_2 + \tau_1 d_1)/(d_2 + d_1) \quad (A.6)$$

Note that $\tau_2 \neq \tau_1$ in the previous expression.

In annuli,

$$A_c = \frac{\pi}{4}(d_2^2 - d_1^2) = \frac{\pi}{4}(d_2 - d_1)(d_2 + d_1) \quad (A.7)$$

and

$$P = \pi(d_2 + d_1) \quad (A.8)$$

Thus, an average wall stress is defined as

$$\tau_{w\,avg} = \left(\frac{\Delta p}{L}\right)\left(\frac{d_2 - d_1}{4}\right) \quad (A.9)$$

Solving for pressure loss

$$\frac{\Delta p}{L} = \left(\frac{4}{d_2 - d_1}\right)\tau_{w\,avg} \quad (A.10)$$

With $\tau_{w\,avg}$ defined by equation (A. 3).

d_1 is the inner diameter and d_2 is the outer diameter of the annulus.

d_2-d_1 in equation (A.9) is the characteristic length (l) in annuli, while in a circular pipe, l = diameter. The characteristic length definition is as follows

$$l = \frac{4\, A_c}{P} \quad (A.11)$$

l is often called the hydraulic diameter and it is involved in Reynolds number (Re) definition as follows

Reynolds number is a dimensionless number which relates inertial to viscous forces and it is useful to characterize flow regime: laminar, transition or turbulent flow in order to predict frictional pressure losses. In turbulent flow characterization, it becomes highly important.

$$Re = \frac{\rho\, v_{avg}\, l}{\mu} \quad (A.12)$$

But Reynolds number is intrinsically related to Newtonian behavior. Viscosity, μ, is not unique in non-Newtonian fluids, because the ratio of shear stress and shear rate is no longer constant as in Newtonian case. This circumstance requires an extension of Reynolds number definition to be applicable in non-Newtonian fluids.

Metzner and Reed (1955) were pioneers in introducing the concept of a generalized Reynolds number for flow of power-law fluids in pipes.

$$Re_g = \frac{d^n\ V_{avg}^{2-n}\ \rho_L}{K'\ 8^{n-1}} \quad (A.13)$$

where,

$$K' = K\left(\frac{3n+1}{4n}\right)^n \quad (A.14)$$

K is the flow consistency index in Pa. s^n and n is the flow behavior index (dimensionless). Equation (A.13) is used

together with (A.18).

From the representation of an annulus as a slot a generalized Reynolds number for flow of power-law fluids in annuli can be defined as

$$\mathrm{Re_g} = \frac{d_e^{n}\, V_{avg}^{2-n}\, \rho_L}{K'\ 12^{n-1}} \tag{A.15}$$

where,

$$K' = K\left(\frac{2n+1}{3n}\right)^{n} \tag{A.16}$$

d_e is any equivalent diameter definition for annuli. $\mathrm{Re_g}$ is commonly referred as $\mathrm{Re_{MR}}$ in honor of the authors mentioned above. Equation (A.15) is used in conjunction with (A.19) for laminar regime, in congruence.

This concept of generalized Reynolds number has been widely used in different closed conduits, annuli included, by inserting the concept of hydraulic diameter or any other equivalent diameter as an attempt to extend the concept of Reynolds number even for turbulent flow. As mentioned above, shear stress and velocity distributions are complex in annuli, the wall stress is not constant along the perimeter and its magnitude differs at the inner and outer walls of the annulus, i.e. $\tau_{w\ \text{inner wall}} \neq \tau_{w\ \text{outer wall}}$.

But, hydraulic diameter is insufficient to accurately correlate geometric effects in turbulent flow as demonstrated for rectangular ducts (Jones, O. C., 1976). It breaks down for rectangular sections of large aspect ratio and, therefore, most probably for annuli with large radius ratio (Guillot and Denis, 1988).

Certainly, there is a need to define an equivalent diameter into the generalized Reynolds number which cares of geometry shape of the annulus into the shear stress and velocity distribution.

We know, that in an annulus the velocity distribution profile depends on the diameter ratio (κ), defined as

$$\kappa = \frac{d_1}{d_2} \tag{A.17}$$

In consequence, the relation of friction factor vs Reynolds number depends also on diameter ratio. It could be

$$(f)(\mathrm{R_e}) \approx 16 \qquad \text{if} \quad \kappa \to 0 \tag{A.18}$$

or

$$(f)(\mathrm{R_e}) = 24 \qquad \text{if} \quad \kappa \to 1 \tag{A.19}$$

Note that when diameter ratio vanishes ($\kappa = 0$), pipe flow exists, i.e. $(f)(\mathrm{R_e}) = 16$ and when $\kappa \to 1$, represents the case of infinite parallel plates (slot) flow, i.e. $(f)(\mathrm{R_e}) = 24$.

Knudsen and Katz (1958) defined a relation between friction factor and Reynolds number as a function of κ in laminar annular flow as follows

$$f = \frac{16}{\mathrm{R_e}}\ \varphi(\kappa) \tag{A.20}$$

here

$$\varphi(\kappa) = \frac{(1-\kappa)^2}{1+\kappa^2+\left[\frac{(1-\kappa^2)}{\ln \kappa}\right]} \tag{A.21}$$

Similar expressions were derived by Bird et al. (1976) and Jones and Leung (1981) to consider the annulus geometry into shear stress and velocity distribution inside of the conduit on friction factor, also known as "shape factor" of the annulus. However, the impact of the shear-thinning behavior is still not included in their expressions. A further evolved definition of equivalent diameter definition, "the effective diameter", considers both effects: the rheological behavior and the annulus geometry.

We can obtain $\varphi(\kappa)$ for any given κ value from equation (A.21) and we can observe that for $0.3 \leq \kappa \leq 1$, the function $\varphi(\kappa)$ varies in the range of $1.466 \leq \varphi(\kappa) \leq 1.5$, it implies that the relation between friction factor and Reynolds number is in the range of $23.46 \leq (\mathrm{F_f})(\mathrm{R_e}) \leq 24$, which is in fair agreement with the representation of plain annuli as parallel plates when κ is bigger than 0.3.

The definition and usage of an equivalent diameter is a common approach when noncircular flow conduits are encountered. The flow behavior in a circular pipe of that 'equivalent diameter' must be consistent to the flow behavior in the noncircular conduit, especially for estimation of total flow rate and pressure losses. Although there are many equivalent diameter definitions available in literature for annular spaces nowadays, e.g. the equivalent diameter derived from the slot approximation (Bourgoyne et al., 1986), no definition is universally accepted. See Table A.1.

$$d_{e\ \text{Slot}} = \sqrt{2/3}\ (d_2 - d_1) \approx 0.81649\ (d_2 - d_1) \tag{A.22}$$

According to Reed and Pilehvari (1993), the "effective" diameter for a non-Newtonian flow through a concentric annulus is the diameter of a circular pipe that would have the identical pressure drop for flow of a Newtonian fluid with a viscosity equal to the "effective" viscosity, which is based on the average wall shear rate in the annulus, and has a velocity equal to the non-Newtonian annular flow velocity. Effective diameter takes information about both conduit geometry and fluid rheology.

The friction factor is a function of the Reynolds number which depends on viscosity and characteristic length. Turbulent friction factors have been empirically derived for pipe flow and Newtonian fluids, basically. A generalized Reynolds number in terms of the non-Newtonian model and flow geometry parameters is commonly used as an approach to employ friction factor correlations developed for pipe flow in an annulus, e.g. the correlation for power-law fluids in concentric smooth annuli, (Dodge and Metzner, 1959).

$$\frac{1}{\sqrt{f}} = \frac{4}{(n')^{0.75}} \log\left[\mathrm{Re_g}\ f^{1-\frac{n'}{2}}\right] - \frac{0.4}{(n')^{1.2}} \tag{A.23}$$

Note that friction factors of power-law fluids depend strongly on flow behavior index, n.

Irvine (1988) provided the following Blasius-like approximate expression to predict friction factor of fully developed turbulent flow of power-law fluids in smooth pipes.

$$f = \left[F(n)/Re_g\right]^{1/(3n+1)} \quad (A.24)$$

where

$$F(n) = \frac{2^{n+4}}{7^{7n}}\left(\frac{4n}{3n+1}\right)^{3\,n^2} \quad (A.25)$$

Note that this expression does reduce to the well-known Blasius expression for n=1; it is explicit in friction factor, f, and it obviates the iterative process needed for the solution of the Dodge and Metzner (1959) correlation for turbulent flow of power-law fluids in terms of Reg.

Other Blasius-type approximate correlations for the friction factor in terms of the behavior index are mentioned in the literature (Jensen and Sharma, 1987; Scheid et al., 2009).

The simplest and most reliable method to define the laminar-to-turbulent transition is to compare pairs of friction factor values: one value computed for turbulent flow and the other value computed for laminar flow, the transition occurs when the friction factor for turbulent flow becomes greater than the friction factor for laminar flow. However, in literature, there are available empirical correlations to estimate the approximate critical value of the Reynolds number for transition from laminar to turbulent flow regime for a pseudo-plastic fluid, e.g. the Ryan and Johnson (1959) criterion

$$Re_g = \frac{6464\,n}{(3n+1)^2}(2+n)^{(2+n)/(1+n)} \quad (A.26)$$

And the Mishra and Tripathi (1975) criterion, among other existing transition criteria.

$$Re_g = \frac{2100\,(4n+2)(5n+3)}{3(3n+1)^2} \quad (A.27)$$

Note that both correlations predict a value of 2100 as critical for Newtonian fluids (n = 1).

Table A.1. Equivalent diameter definitions for annuli

#	Expression		
1	$D = 2\sqrt{r_o^2 + r_i^2 - r_m^2}$ Where $r_m^2 = \frac{r_o^2 - r_i^2}{2.3\log(r_o/r_i)}$	Lohrenz and Kurata (1960)	
2	$d_h = \frac{4\,A}{P} = d_2 - d_1$	Hydraulic diameter	
3	$d_c = 0.5\left[d_o^4 - d_i^4 - \frac{\left(d_o^2 - d_i^2\right)^2}{\ln(d_o/d_i)}\right]^{0.25} + 0.5\left(d_o^2 - d_i^2\right)^{0.5}$	Crittendon (1959)	Empirical from statistics of field pump pressures
4	$d_s = \sqrt{\frac{2}{3}}\ (d_o - d_i) \approx 0.816\,(d_o - d_i)$	Slot approximation Bourgoyne et al. (1986)	
5	$D_{e,p} = \sqrt[5]{(d_o + d_i)^2(d_o - d_i)^3}$	The petroleum diameter	
6	$D_{e,a} = \left(d_o^2 - d_i^2\right)^{1/2}$	The equivalent area diameter	Also known as the representative diameter (d_R).
7	$D_{e,g} = \sqrt{d_o^2 + d_i^2 - \frac{d_o^2 - d_i^2}{\ln(d_o/d_i)}}$	Lamb approach (1945)	
8	$d_e = d_o(1-\kappa)\varphi$ Where $\varphi = \frac{1}{1-\kappa^2}\left[(1+\kappa^2) - \frac{1-\kappa^2}{\ln(1/\kappa)}\right]$	Meter and Bird (1961)	Similar to Jones and Leung (1981) and to Knudsen and Katz (1958)
9	$d_{eq} = d_o + d_i$	The equi-peripheral diameter. Sadatomi et al. (1982).	Wetted perimeter of the channel divided by π. Equal to the sum of the annuli diameters. For two-phase flow in annuli.
10	$d_{eff} = \frac{1}{2}\left[\frac{\pi(d_o + d_i)}{2} + \frac{d_o - d_i}{2}\right] = \frac{1}{4}\left[(\pi+1) + \frac{d_i}{d_o}(\pi - 1)\right]$	The "effective" diameter. Barnea and Shemer (1986)	To evaluate the rising velocity of a Taylor bubble in annuli based on the mean of the gap width and the gap circumference.
11	$d_e = \frac{d_o - d_i}{G}$ With $G = (1 + Z/2)\,[(3-Z)n + 1]/[(4-Z)n]$ $Z = 1 - [1 - (d_i/d_o)^Y]^{1/Y}$ $Y = 0.3n^{-0.14}$	Effective diameter for power-law fluids annuli. Reed and Pilehvari (1993)	As a function of the annular geometry and rheology fluid (power-law).
12	$d_{eff,PL,Conc} = \frac{\beta\ d_2^{3+1/n}}{(d_2 + d_1)\ (d_2 - d_1)^{1+1/n}}$ With $\beta = (1+\kappa)(1-\kappa)^{\frac{1}{n}+2}\left[1 - \frac{1}{93}n^{-\frac{5}{9}}\left(\frac{1}{\kappa} - 1\right)^{\frac{9}{10}}\right]^{-1}$ $Re_{g,PL,Conc} = \frac{v_{avg}^{\,2-n}\ \rho\ d_{eff,PL,Conc}^{\,n}}{12^{n-1}\,g_c\,K\left(\frac{2n+1}{3n}\right)^n}$	Effective diameter for power-law fluids in annuli. Dosunmu and Shah (2015)	From a quasi-similarity approximate solution (David and Filip, 1995) of the exact solution of Fredrickson and Bird (1958). Eliminates iterative calculation of Pilehvari and Serth (2009)